trend in Fig. 4 seems linear and through the origin, in the literature, several individual data sets suggest[5] the following: 1) a nonlinear trend and 2) a drag reduction as $f \to 0$. Such a behavior would be reminiscent of riblets.[18] However, the scatter in Fig. 4 is too large to resolve these possibilities. Further research with pressure gradients and curvature should be carried out to determine the applicability of the flat plate results to the turbomachine flow problem.

Conclusions

The published experimental data on the influence of freestream turbulence on turbulent boundary layers have been examined to determine the effect of Reynolds number on such influence. Two manifestations of the effect of low Reynolds numbers on the outer layer are observed. First, the Clauser's shape parameter G is Reynolds number dependent at very low Reynolds numbers. Second, the reduction in the wake component due to freestream turbulence undergoes a *reversal* in the Reynolds number dependence depending on the value of the freestream turbulence parameter. Hancock's freestream turbulence parameter has been modified using these observations. This has led to a new correlation of the fractional increase in skin friction due to freestream turbulence.

Acknowledgment

The financial support of NASA (NAS1-19320) is gratefully acknowledged.

References

[1]Robertson, J. M., and Holt, C. F., "Stream Turbulence Effects on the Turbulent Boundary Layer," *Proceedings of the ASCE*, Vol. 98, HY6, 1972, p. 1093.

[2]Green, J. E., "On the Influence of Free Stream Turbulence on a Turbulent Boundary Layer, as it Relates to Wind Tunnel Testing at Subsonic Speeds," Fluid Motion Problems in Wind Tunnel Design, AGARD Rept. 602, 1973, pp. 4.1-4.8.

[3]McDonald, H., and Kreskovsky, J. P., "Effect of Free Stream Turbulence on the Turbulent Boundary Layer," *International Journal of Heat and Mass Transfer*, Vol. 17, No. 7-A, 1974, pp. 705-716.

[4]Hancock, P. E., "The Effect of Free-Stream Turbulence on Turbulent Boundary Layers," Ph.D. Dissertation, Imperial College, London, 1980.

[5]Hancock, P. E., and Bradshaw, P., "The Effect of Free-Stream Turbulence on Turbulent Boundary Layers," *Transactions of the ASME, Journal of Fluids Engineering*, Vol. 105, Sept. 1983, pp. 284-289.

[6]Castro, I. P., "Effects of Free Stream Turbulence on Low Reynolds Number Boundary Layers," *Transactions of the ASME, Journal of Fluids Engineering*, Vol. 106, Sept. 1984, pp. 298-306.

[7]Blair, M. F., "Influence of Free-Stream Turbulence on Turbulent Boundary Layer Heat Transfer and Mean Profile Development, Part II—Analysis of Results," *Transactions of the ASME, Journal of Heat Transfer*, Vol. 105, Feb. 1983, pp. 41-47.

[8]Blair, M. F., and Werle, M. J., "The Influence of Free-Stream Turbulence on the Zero Pressure Gradient Fully Turbulent Boundary Layer," United Technologies Research Center, Rept. R80-914388-12, Sept. 1980.

[9]Meier, H. U., and Krepline, H. P., "Influence of Free-Stream Turbulence on Boundary Layer Development," *AIAA Journal*, Vol. 18, No. 1, 1980, pp. 11-15.

[10]Huffman, G. D., Zimmerman, D. R., and Bennett, W. A., "The Effect of Free-Stream Turbulence Level on Turbulent Boundary Layer Behaviour," *Boundary Layer Effects in Turbomachines*, AGARDograph 164, 1972, pp. 91-115.

[11]Charnay, G., Comte-Bellot, G., and Mathieu, J., "Development of Turbulent Boundary Layer on a Flat Plate in an External Turbulent Flow," AGARD CP 93, 1971, pp. 27.1-27.10.

[12]Epik, E. Y., and Rumyantseva, L. A., "Characteristics of Turbulent Boundary Layers at High Free-Stream Turbulence," *Fluid Mechanics-Soviet Research*, Vol. 7, No. 3, 1978, pp. 85-90.

[13]Bandyopadhyay, P. R., and Ahmed, A., "Turbulent Boundary Layers Subjected to Multiple Curvatures and Pressure Gradients," *Journal of Fluid Mechanics* (submitted for publication).

[14]Bandyopadhyay, P. R., "Rough-Wall Turbulent Boundary Layers in the Transition Regime," *Journal of Fluid Mechanics*, Vol. 180, 1987, pp. 231-266.

[15]Anders, J. B., "Boundary Layer Manipulators at High Reynolds Numbers," *Structure of Turbulence and Drag Reduction*, edited by A. Gyr, IUTAM Symposium, Zurich, 1989, Springer-Verlag, New York, pp. 475-482.

[16]Gillis, J. C., "Turbulent Boundary Layer on a Convex, Curved Surface," Ph.D. Dissertation, Mechanical Engineering Dept., Stanford Univ., Stanford, CA, 1980.

[17]Bandyopadhyay, P. R., " Resonant Flow in Small Cavities Submerged in a Boundary Layer," *Proceedings of the Royal Society of London, Series A*, Vol. 420, 1988, pp. 219-245.

[18]Walsh, M. J., "Riblets," *Viscous Drag Reduction in Boundary Layers*, edited by D. M. Bushnell and J. N. Hefner, Vol. 123, Progress in Astronautics and Aeronautics, AIAA, Washington, DC, 1990, pp. 203-261.

Analysis of Damping in Composite Laminates

R. Maaskant* and J. S. Hansen†
University of Toronto,
Downsview, Ontario M3H 5T6, Canada

I. Introduction

AMONG the virtues of fiber-reinforced composite materials are relatively high-damping characteristics, an attractive feature for vibration control in lightweight structures. This enhanced damping capacity originates from the viscoelastic behavior of the constituent components, usually the matrix, but in some cases also the fibers. Other sources of damping resulting from damaged or debonded composites and large vibration amplitudes are not considered here.

Viscoelastic materials under steady-state vibration can be characterized by complex stiffness and compliance coefficients,[1] manifested by the experimentally observed phase lag between stress and strain. According to the viscoelastic correspondence principle, these complex coefficients may be used directly in the equations of elastic analysis. The dynamic behavior, including damping, can therefore be characterized according to laminate theory.[2] This approach has been used to evaluate the damping capacity of composite laminates based on experimental data from beam bending and torsion experiments (see, e.g., Refs. 3 and 4). The damping capacity has also been analyzed using a strain-energy approach according to the analysis of Ungar and Kerwin,[5] whereby the components of the dissipated energy are assigned to be a fraction of the corresponding components of the strain energy (see, e.g., Refs. 6-8). As will be seen later, the difficulty with this approach is that these strain-energy components are not independent in the context of the material constitutive relation, which is in contrast with the array of independent springs of the analysis of Ungar and Kerwin.[5] Thus, the manner in which the method is applied has implications with regard to its accuracy for general states of strain.

In the present study, these two approaches are compared to address the apparent discrepancy between them and to evaluate the significance of this discrepancy for a typical composite laminate material. For problems of uniaxial stress, beam bending, and pure shear, addressed by the studies described earlier, the two formulations give essentially the same results. Herein, more general states of strain are considered for which a relative difference in specific damping capacity of up to 8% is obtained.

Received Aug. 5, 1991; revision received Oct. 10, 1991; accepted for publication Oct. 18, 1991.

*Research Associate, Institute for Aerospace Studies, 4925 Dufferin Street.

†Professor, Institute for Aerospace Studies, 4925 Dufferin Street.

II. Energy Storage and Dissipation

The behavior of viscoelastic composites in harmonic steady-state vibration can be described by the complex constitutive relations[1]

$$\sigma_0^* = Q^* \epsilon_0^*, \qquad \epsilon_0^* = S^* \sigma_0^* \tag{1}$$

where σ_0^* and ϵ_0^* are related to the time-domain stresses and strains by

$$\sigma(t) = \Re[\sigma_0^* \exp(i\omega t)], \qquad \epsilon(t) = \Re[\epsilon_0^* \exp(i\omega t)] \tag{2}$$

Complex quantities are herein denoted by a superscript asterisk, $\Re$ denotes the real part of a complex quantity, and $i = \sqrt{-1}$. The complex stiffness matrix Q^* and complex compliance matrix S^* may be written in the alternate forms

$$Q_{jk}^* = Q_{jk}' + iQ_{jk}'' = Q_{jk}'(1 + i\eta_{jk}) \tag{3}$$

$$S_{jk}^* = S_{jk}' - iS_{jk}'' = S_{jk}'(1 - i\zeta_{jk}) \tag{4}$$

The stress (strain) components are in general out of phase, and from Eqs. (1), it can be seen that this phase difference is stress/strain dependent.

The mechanical energy absorbed by a material (per unit volume) is given by

$$\mathcal{U} = \int \sigma^T(t)\, \mathrm{d}\epsilon(t) \tag{5}$$

and this consists of energy stored $\mathcal{U}_s$ and energy dissipated $\mathcal{U}_d$. Since there is no net energy stored over a complete cycle in steady-state vibration, the energy dissipated per cycle can be calculated as

$$\mathcal{U}_d = \int_0^{2\pi/\omega} \sigma^T(t)\dot{\epsilon}(t)\, \mathrm{d}t = \pi \Im[\sigma_0^{*T} \bar{\epsilon}_0^*] \tag{6}$$

in which an overbar represents the complex conjugate and $\Im$ denotes the imaginary part of a complex quantity. Written in terms of strain this becomes

$$\mathcal{U}_d = \pi \Im[\epsilon_0^{*T} Q^* \bar{\epsilon}_0^*] \approx \pi \epsilon_0^T Q'' \epsilon_0 \tag{7}$$

The latter approximate form is valid for low damping ($\eta_{ij} \ll 1$). The maximum energy stored in a cycle is required for the calculation of the specific damping capacity. It cannot be so easily calculated, but is generally taken as

$$\mathcal{U}_s = \left| \int_0^{\pi/2\omega} < \sigma^T(t)\dot{\epsilon}(t) > \mathrm{d}t \right| \tag{8}$$

where the angle brackets denote those components of the integrand of Eq. (5) that do not contribute to the dissipated energy $\mathcal{U}_d$. The result is actually the maximum coherently storable energy,[9] i.e., that which could be stored if all storage mechanisms are in phase (strictly valid only in the elastic case and approximately valid for low damping). Making the appropriate substitutions into Eq. (8), the maximum stored energy is given by

$$\mathcal{U}_s = \tfrac{1}{2} \Re[\sigma_0^{*T} \bar{\epsilon}_0^*] \approx \tfrac{1}{2} \epsilon_0^T Q' \epsilon_0 \tag{9}$$

These expressions can be used to calculate the specific damping capacity, which is defined as the ratio of the dissipated energy to the maximum stored energy over one cycle of vibration

$$\psi = \frac{\int_\mathcal{V} \mathcal{U}_d \mathrm{d}\mathcal{V}}{\int_\mathcal{V} \mathcal{U}_s \mathrm{d}\mathcal{V}}$$

where the integration is performed over the volume $\mathcal{V}$.

According to the alternative strain-energy approach, the dissipated energy is separated into three parts corresponding

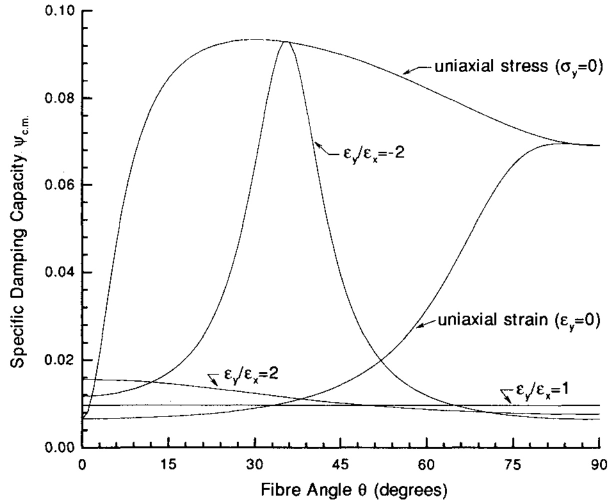

Fig. 1 Variation of specific damping capacity for unidirectional lamina (θ positive counterclockwise from x axis).

to each of the three components of the strain energy, i.e.,

$$\mathcal{U}_d = \tfrac{1}{2}[\psi_1 \sigma_1 \epsilon_1 + \psi_2 \sigma_2 \epsilon_2 + \psi_6 \sigma_6 \epsilon_6] \tag{10}$$

The remaining components, arising from interlaminar stresses, are here ignored since these are essentially independent of the others and will not contribute to the difference between the two formulations under consideration. The stresses and strains indicated are the magnitudes of their cyclic counterparts and are referred to the lamina principle axes. The values of the component specific damping capacities ψ_1, ψ_2, ψ_6 are often established by flexural and torsional tests on beam specimens.

Returning now to the complex formulation, the complex stress and strain quantities σ_0^* and ϵ_0^* can be written as

$$\sigma_0^* = \mathrm{diag}[\exp(i\phi)]\sigma_0, \qquad \epsilon_0^* = \mathrm{diag}[\exp(i\xi)]\epsilon_0 \tag{11}$$

where the phase matrices are of the form

$$\mathrm{diag}[\exp(i\phi)] = \begin{bmatrix} \exp(i\phi_1) & 0 & 0 \\ 0 & \exp(i\phi_2) & 0 \\ 0 & 0 & \exp(i\phi_6) \end{bmatrix} \tag{12}$$

and the vectors σ_0 and ϵ_0 contain the magnitudes of the complex stress and strain components. Substituting into Eq. (6) gives

$$\mathcal{U}_d = \pi \sigma_0^T \Im \begin{bmatrix} \exp[i(\phi_1 - \xi_1)] & 0 & 0 \\ 0 & \exp[i(\phi_2 - \xi_2)] & 0 \\ 0 & 0 & \exp[i(\phi_6 - \xi_6)] \end{bmatrix} \epsilon_0 \tag{13}$$

According to Eq. (10), the two formulations are equivalent only if

$$\psi_j = 2\pi \Im\{\exp[i(\phi_j - \xi_j)]\} \tag{14}$$

From this, it may be concluded that the specific damping capacities ψ_j are stress/strain dependent, or more precisely, they are dependent on the phase lag between stress and strain. Therefore, the definition of constant ψ_j values is inconsistent with the damping characteristics of a complex modulus material.

The form of the matrices Q^* and S^* implied by Eq. (10) is easily derived by comparison of the respective dissipated energy expressions. For low damping, this gives the effective loss factor matrices[10]

$$\eta = \zeta = \frac{1}{2\pi}\begin{bmatrix} \psi_1 & \frac{1}{2}(\psi_1+\psi_2) & 0 \\ \frac{1}{2}(\psi_1+\psi_2) & \psi_2 & 0 \\ 0 & 0 & \psi_6 \end{bmatrix} \tag{15}$$

Two observations can be made. First, the implied equality between the loss factor matrices corresponding to Q^* and S^* is incorrect; second, the Poisson coupling term cannot be of this form for a general orthotropic material. Thus, one can conclude that the dissipated energy calculated on this basis cannot be correct for a general state of stress or strain. It may be expected that such results will be acceptable for stress/strain states similar to those experienced experimentally in the determination of the ψ_j terms.

Since the values of ψ_1 and ψ_2 are generally determined under conditions of uniaxial stress, i.e., beam flexure or tension, these may be used to calculate the complex engineering constants according to

$$E_1^* = E_1\left(1 + i\frac{\psi_1}{2\pi}\right) \tag{16}$$

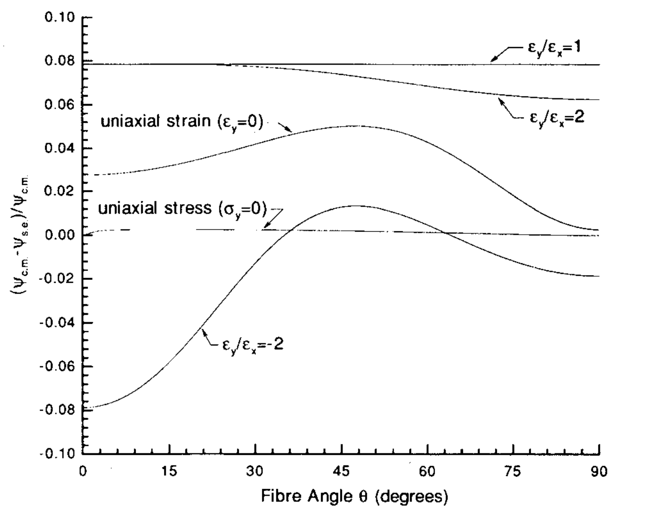

Fig. 2 Deviation of the specific damping capacity for unidirectional lamina.

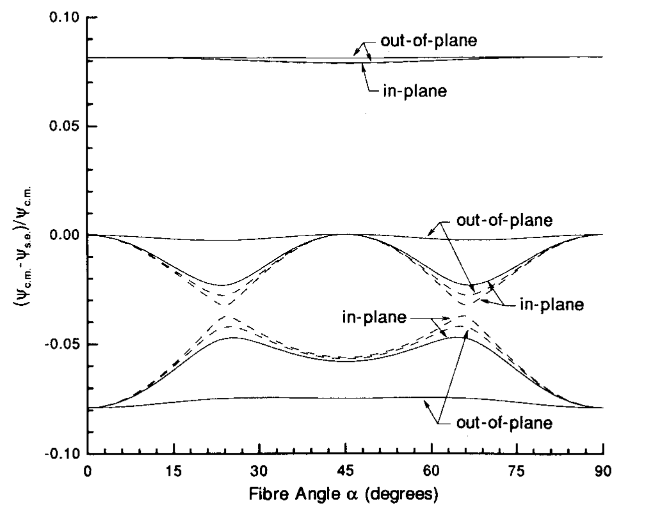

Fig. 3 Maximum deviation of the specific damping capacity for regular symmetric angle-ply laminates. Three layers: solid lines; 15 layers: dashed lines.

Table 1 Maximum deviation of the specific damping capacity for various laminates

Layup	Maximum relative deviation $(\psi_{cm} - \psi_{se})/\psi_{cm}$
Unidirectional	+ 8.15, − 7.89
Quasi-isotropic	
$[-60, 0, 60]_s$	+ 7.96, − 5.16
$[0, -45, 45, 90]_s$	+ 7.97, − 4.20
Symmetric cross ply	
[0, 90, 0]	+ 8.10, − 7.48
[0, 90, 90, 0]	+ 8.01, − 6.75
[0, 90, 0, 90, 0]	+ 7.94, − 6.27
[0, 90, 0, 90, 0, 90, 0, 90, 0]	+ 7.87, − 5.82
Unsymmetric cross ply	
[0, 90]	+ 8.06, − 7.20
[0, 90, 0, 90, 0, 90, 0, 90]	+ 7.85, − 5.65

$$E_2^* = E_2\left(1 + i\frac{\psi_2}{2\pi}\right) \tag{17}$$

$$G_{12}^* = G_{12}\left(1 + i\frac{\psi_6}{2\pi}\right) \tag{18}$$

In the absence of further experimental data, ν_{12} is taken to be real in accordance with the simple rule of mixtures formula and the usual assumption that the Poisson's ratio of the viscoelastic matrix is real.[1]

The usual elastic relations can be used to calculate Q_{ij}^*, yielding the loss factors

$$\eta_{11} = \frac{1}{2\pi}\left[\psi_1 + \frac{\nu_{12}^2 E_2}{E_1 - \nu_{12}^2 E_2}(\psi_2 - \psi_1)\right] \tag{19}$$

$$\eta_{22} = \frac{1}{2\pi}\left[\psi_2 + \frac{\nu_{12}^2 E_2}{E_1 - \nu_{12}^2 E_2}(\psi_2 - \psi_1)\right] \tag{20}$$

$$\eta_{12} = \eta_{22} \tag{21}$$

$$\eta_{66} = \frac{\psi_6}{2\pi} \tag{22}$$

wherein only first-order terms in the small quantities ψ_i are retained.

III. Some Numerical Results

Damping calculations for an example unidirectional composite material are now presented. Material data is taken from the study of Adams and Bacon[6] as summarized in the following (HM-S carbon fibers in DX209 epoxy matrix, volume fraction = 0.5):

$$E_1 = 188.9 \text{ GPa}, \quad E_2 = 6.081 \text{ GPa}, \quad G_{12} = 2.723 \text{ GPa}$$

$$\nu_{12} = 0.3, \quad \psi_1 = 0.64\%, \quad \psi_2 = 6.9\%, \quad \psi_6 = 10\%$$

The specific damping capacity is calculated using both the strain-energy approach ψ_{se} and the complex modulus approach ψ_{cm}, and comparisons are made for various layups and states of strain.

The specific damping capacity for a unidirectional lamina in various states of strain is given in Fig. 1 for fiber angles θ. The difference relative to the specific damping capacity from the complex modulus approach is shown in Fig. 2. For a uniaxial state of stress, the difference in the two approaches is very small, and they are identical in the 0- and 90-deg directions since these correspond to the experimental states of stress. In the case of uniaxial strain, a deviation of up to 5% occurs, but it becomes small for $\theta = 0$ and 90 deg. The deviation can be seen to be strongly dependent on the state of strain.

The maximum relative deviation in ψ for any particular lay-up can be obtained by extremizing the ratio $\lambda = \psi_{se}/\psi_{cm}$. This results in the eigenvalue problem

$$\left(\begin{bmatrix} A'' & B'' \\ B'' & D'' \end{bmatrix}_{se} - \lambda \begin{bmatrix} A'' & B'' \\ B'' & D'' \end{bmatrix}_{cm}\right)\begin{Bmatrix} \epsilon_m \\ \kappa \end{Bmatrix} = 0 \tag{23}$$

where the double primed quantities are the imaginary part of the (complex) stiffness matrices $\boldsymbol{A}^*$, $\boldsymbol{B}^*$, and $\boldsymbol{D}^*$ of classical laminated plate theory,[2] and ϵ_m and κ are the amplitudes of the cyclic midplane strains and curvatures, respectively. This has been solved for a number of different laminates and the results are summarized in Table 1 and Fig. 3. The maximum relative difference $(1 - \lambda)$ has magnitudes as high as $\pm 8\%$ and is weakly dependent on the laminate layup. As can be seen in Fig. 3, the extremal deviations for regular symmetric angle-ply laminates occur in pairs for which the corresponding displacements are in-plane and out-of-plane, respectively. Although the state of strain is not constant over α, it can be characterized approximately as equal biaxial strain/curvature, pure shear/twist, and unequal biaxial strain/curvature for the upper, middle, and lower pairs of curves of Fig. 3, respectively. Similar trends were observed for the layups given in Table 1.

IV. Conclusions

The damping capacity of fiber-reinforced composite laminates has been calculated for general states of strain using the complex modulus approach and an alternative approach based on the components of the strain energy. It has been shown that the formulations are inconsistent with each other, although for the case of uniaxial stress the calculated differences are negligible. For more general states of strain, maximum discrepancies of approximately $\pm 8\%$ were found for a wide range of (carbon-epoxy) laminates. The discrepancy in any particular case is strongly dependent on the laminate configuration and the state of strain.

References

[1]Schapery, R. A., "Viscoelastic Behavior and Analysis of Composite Materials," *Mechanics of Composite Materials*, Vol. 2, Academic, New York, 1974, pp. 85–168.

[2]Jones, R. M., *Mechanics of Composite Materials*, Hemisphere, New York, 1975.

[3]Schultz, A. B., and Tsai, S. W., "Measurements of Complex Dynamic Moduli for Laminated Fiber-Reinforced Composites," *Journal of Composite Materials*, Vol. 3, July 1969, pp. 434–443.

[4]Gibson, R. F., and Plunkett, R., "Dynamic Mechanical Behavior of Fiber-Reinforced Composites: Measurement and Analysis," *Journal of Composite Materials*, Vol. 10, Oct. 1976, pp. 325–341.

[5]Ungar, E. E., and Kerwin, E. M., "Loss Factors of Viscoelastic Systems in Terms of Energy Concepts," *Journal of the Acoustical Society of America*, Vol. 34, No. 7, 1962, pp. 954–957.

[6]Adams, R. D., and Bacon, D. G. C., "Effect of Fiber Orientation and Laminate Geometry on the Dynamic Properties of CFRP," *Journal of Composite Materials*, Vol. 7, Oct. 1973, pp. 402–428.

[7]Saravanos, D. A., and Chamis, C. C., "Unified Micromechanics of Damping for Unidirectional and Off-Axis Fiber Composites," *Journal of Composites Technology and Research*, Vol. 12, No. 1, 1990, pp. 31–40.

[8]Hwang, S. J., and Gibson, R. F., "The Effects of Three-Dimensional States of Stress on Damping of Laminated Composites," *Composites Science and Technology*, Vol. 41, No. 4, 1991, pp. 379–393.

[9]Tschoegl, N. W., *The Phenomenological Theory of Linear Viscoelastic Behavior*, Springer-Verlag, New York, 1989, p. 454.

[10]Morison, W. D., "The Effects of Moisture Loss and Elevated Temperature upon the Material Damping of Fiber Reinforced Polymer Matrix Composites," Inst. for Aerospace Studies, Univ. of Toronto, Rept. 324, Ontario, Canada, July 1988.

Separated High Enthalpy Dissociated Laminar Hypersonic Flow Behind a Step—Pressure Measurements

S. L. Gai*

University of New South Wales,
Australian Defence Force Academy,
Campbell, ACT 2600, Australia

Introduction

THE impetus for the current resurgence of interest in hypervelocity flows is the increased activity in the area of space technology such as the reusable space planes, for example, the National Aero-Space Plane or NASP (United States), the HOTOL (United Kingdom), the HERMES (France), and the SÄNGER (Germany).

The design and development of these space vehicles, which operate at high velocity and high altitudes, make it imperative that detailed knowledge of the flowfield around such bodies is known. However, such data are still sparse, especially with respect to separating and reattaching flows. The separating and reattaching flow phenomenon is important because it may affect the control effectiveness and maneuverability of the vehicle or the propulsion/instrumentation unit may be located in the lee of the vehicle (e.g., the aeroassist flight experiment vehicle).

During the sixties a number of analytical and experimental separated and wake flow studies at both supersonic and hypersonic speeds were conducted.[1-7] These studies provided detailed insight and understanding into the behavior of separated flows with the separating boundary layer either laminar or turbulent. However, they dealt with only undissociated perfect gas with $\gamma = 1.4$. Not much information is available, therefore, pertaining to the behavior of separated flow at hypervelocities and under high enthalpy conditions at which the proposed space vehicles will operate.

In a recent study, Gai et al.[8] investigated laminar separated flow behind a two-dimensional backward-facing step in dissociated high enthalpy hypervelocity stream using a free-piston driven shock tunnel (FPST) that generates velocities and enthalpies experienced during the flight of aeroassisted space transfer vehicles (ASTVs). In that study, measurement of heat transfer and flow visualization using Mach-Zehnder interferometry were made and the importance of flow geometry and Reynolds numbers investigated. In the present Note, we describe pressure measurements made with the same model under similar flow conditions. To the author's knowledge, no data obtained under such high enthalpy hypervelocity flow conditions are currently available. This study is thus complementary to that described in Ref. 8.

Experiments

The experiments were conducted in the Australian National University free-piston driven shock tunnel T3[9] that can generate stagnation enthalpies and temperatures in air equivalent to those experienced by ASTVs. Under those conditions, dissociation of oxygen and nitrogen molecules can occur. The dissociated test gas in the reservoir at the end of the shock tube that is in chemical equilibrium and vibrationally fully excited is expanded through a hypersonic nozzle. As the gas expands through the nozzle, vibrational de-excitation and chemical

Received May 20, 1991; revision received Sept. 20, 1991; accepted for publication Nov. 1, 1991.

*Senior Lecturer, Mechanical Engineering Department, University College. Associate Fellow AIAA.